Multivariable Fuzzy Logic Controlled Photothermal Therapy

Mauricio Céspedes Tenorio * **Diego S. Dumani** *

* *Biomedical Engineering Research Laboratory, School of Electrical Engineering Universidad de Costa Rica, San Pedro, San José, Costa Rica*

Abstract: Photothermal therapy has emerged as a potential modality to generate hyperthermia as cancer treatment due to its low invasiveness and its capacity to complement other cancer therapies. Undesired side effects can occur such as damage to surrounding healthy tissue and temperature increase to values that cause tissue carbonization and evaporation. For this reason, this research aims to develop a multivariable fuzzy logic controller that maximizes tumor thermal damage while keeping temperature within the recommended ranges and minimizing neighboring healthy tissue damage. Three inputs were contemplated for the control system: tumor thermal damage, future maximum temperature error and future healthy tissue temperature error; thirteen logic rules were used to determine the controller output, which was established to be the change in laser power. Results showed that the control algorithm successfully accomplished the proposed goals.

Keywords: Decision support systems and feedback control, intensive and chronic therapy, biomedical system modelling, hyperthermia, photothermal therapy, biomedical imaging systems, simulation and visualization.

1. INTRODUCTION

Cancer is one of the most important causes of death worldwide, leaving around 18.1 millions new patients and 9.6 millions deaths in 2018 (International Agency for Research on Cancer, 2003).

Despite the advances in cancer treatment during recent decades, effort is still needed to improve therapy efficiency and reduce side effects (Rehman, 2018; National Cancer Institute, 2015). Some of the most common therapies include surgery, chemotherapy, and radiotherapy. Novel types of therapies have also emerged as a complement to the already existing ones.

Hyperthermia has been widely studied as an alternative or complement to conventional treatments. This type of therapy is based in a local increase in tissue temperature that causes thermal damage and apoptosis (death) of cancer cells (Instituto Nacional del Cáncer, 2011; Manzoor and Dewhirst, 2011; Shaikh et al., 2013). These temperatures are usually close to 45 °C; however, it is also possible to use temperatures above 46 °C, which is known as hyperthermic ablation. Moreover, it has been found that exposing mammalian cells to temperatures above 60 °C originates rapid protein denaturation and also melts the plasma membrane, causing irreversible cell damage (Chris Brace, 2008).

Photothermal therapy (PTT) is a type of hyperthermia that uses a laser to generate heat (Chen et al., 1995). Due to its minimal invasiveness and potential to complement other cancer treatments, PTT is an attractive option to implement clinically (Ge et al., 2019). Nevertheless, PPT is not exempt of side effects such as damage of neighboring tissue. Additionally, temperatures in excess of 105 °C can cause tissue carbonization and evaporation (Dombrovsky et al., 2011; Long et al., 2019). Therefore, the temperature must be high enough to generate irreversible damage to the tumor, but without damaging surrounding healthy tissue or exceeding the recommended range.

In this investigation, we propose the integration of a fuzzy logic controller (FLC) coupled with a photothermal therapy system. The main objective is to reduce surrounding healthy tissue damage, to avoid tissue carbonization and evaporation, and to maximize tumor damage (thus, therapy efficiency). To address this purpose, a fuzzy logic controller and a photothermal therapy simulation were developed in MATLAB®. Both systems were subsequently integrated to test the controller performance.

The simulation assumes that real-time 3D temperature measurements are available. In a clinical setting, this could be achieved non-invasively via either ultrasound or photoacoustic imaging, which have been shown capable of real-time temperature guidance during hyperthermia (Shah et al., 2008a,b).

2. METHODS

2.1 Mathematical modelling for photothermal therapy

Temperature distribution in tissue The behavior of heat diffusion in the tissue is governed by the Pennes bioheat equation (Ren et al., 2017; Douplik, 2014; Pennes, 1948):

⋆ This work was supported by the University of Costa Rica under grants C0232 and C1464.

$$\rho c_p \frac{\partial T}{\partial t} = k\nabla^2 T + Q \tag{1}$$

where ρ is the mass density, c_p is the specific heat, k is the thermal conductivity. These last three properties change according to tissue type. T is temperature and Q represents the heat source, which is given by (Ren et al., 2017; Douplik, 2014):

$$Q = Q_M + Q_S + Q_L \tag{2}$$

where Q_M and Q_S represent the metabolic heat generation rate and the heat transfer from the blood, respectively. Q_L stands for the heat rate generated by the external light source, i.e., the laser. Q_S term can be calculated by Equation 3, where W is the mass flow rate of blood per unit of volume of tissue (which varies according to tissue type) and, c_s and T_s are the blood specific heat and temperature, respectively (Kengne et al., 2012).

$$Q_S = c_s W(T_s - T) \tag{3}$$

The metabolic heat rate Q_M cannot be described by one particular equation; therefore, its value should be approximated according to literature reported data (Ren et al., 2017). Lastly, the term that requires the most complex calculations is Q_L because of its dependence on tissue light absorption. Generally, it is given by (Jacques and Health, 1995):

$$Q_L = \mu_a \phi \tag{4}$$

where μ_a is the absorption coefficient of the medium and ϕ is the local light fluence. The only heat rate responsible of hyperthermia is Q_L, while Q_M and Q_S represent physiological mechanisms that regulate body temperature.

The mathematical model of tissue temperature was implemented using finite element analysis, as part of MATLAB's Partial Differential Equation (PDE) Toolbox.

Light propagation in tissue Monte Carlo method was used to estimate the light fluence (ϕ) distribution in tissue. This technique is based on dividing the geometry of the tissue of interest into finite elements and simulating the light propagation as the movement of photon packets within the structure, until these packets abandon the considered spatial limits or are completely absorbed. The model accounts for optical phenomena including reflection, refraction, scattering and absorption (Prahl, 1988; Jacques and Health, 1995).

The open source code *ValoMC* was utilized in MATLAB® to simulate light propagation. This program implements the Monte Carlo method for light passage in biological tissue, both in 2D and 3D (Leino et al., 2019).

Tissue thermal damage Thermal damage was quantitatively approximated through Arrhenius equation (Ren et al., 2017; Pearce, 2011, 2018):

$$\zeta(x,y,z,t) = \int_0^{\tau} A \exp\left(-\frac{\Delta E_a}{R \cdot T(x,y,z,t)}\right) dt \qquad \forall\ t : 0 < t < \tau \tag{5}$$

where ζ is the damage coefficient, A is the frequency factor, ΔE_a is the activation energy, R is the gas constant ($8.314\,\mathrm{J \cdot mol^{-1}K^{-1}}$), T stands for temperature and τ is the exposure time. Assuming that thermal damage equals zero at time zero, the percentage of thermal damage can be calculated as follows (Paruch, 2020; Soni et al., 2015):

$$P(x,y,z,t) = 100[1 - \exp(-\zeta(x,y,z,t))] \tag{6}$$

2.2 Controller design

Other studies have proposed the use of different control algorithms for hyperthermia treatments, such as PID, POF, adaptive control or MPC (Sun et al., 2005; Jeraldin Auxillia, 2015; VanBaren et al., 1995; Deenen et al., 2018). For photothermal therapy, specifically, PID and fuzzy logic schemes have been implemented; however, these studies only took into consideration the temperature of tissue and related measurements, such as temperature increase rate vs. time (Chen et al., 2019; Nguyen et al., 2016; Choy et al., 2002). In this research, the aim is to design a closed-loop controller not only for the specific tissue model, but also for diverse tissues with variations such as tumor depth, size or location (only restricted by light penetration and distribution limitations). For this reason and in order to manage the nonlinear behavior of the process and its mathematical model, a closed-loop fuzzy logic controller (FLC) was designed and coupled with the PTT system.

Another difference of the controller presented in this paper is that it would allow the physician to decide temperature setpoints, both inside the tumor and in surrounding healthy tissue. Therefore, this control scheme is more capable to be adjusted in agreement with the physician judgment about the specific patient characteristics. Additionally, thermal damage estimation is considered in the rules of the control system, which was not found in any of the related previous studies for PTT.

In our study, the FLC has three main purposes: maximize tumor thermal damage, thus, effectiveness of PTT; minimize surrounding healthy tissue thermal damage; and to keep temperature between recommended ranges, i.e., high enough to cause ablation without exceeding 105 °C (which causes tissue evaporation and carbonization). Additionally, three error inputs were considered for the FLC, which are:

→ Error in tumor thermal damage percentage ($e_{TD,tumor}$): Estimated from the lowest temperature measurement inside the tumor ($T_{tumor,min}$), associated with the least damaged region. This is calculated from Equations 5 and 6 as follows:

$$e_{TD,tumor} = 100\% - P(\%) \tag{7}$$

→ Future error in the tumor highest temperature ($e_{T,max}$): To obtain this information, the future highest temperature inside the tumor is calculated from two temperature measurements as follows:

$$T_{max}(t+1) = 2T_{max}(t) - T_{max}(t-1) \tag{8}$$

where $T_{max}(t+1)$ is the future value of the tumor highest temperature, $T_{max}(t)$ is the current value of the tumor highest temperature measurement and $T_{max}(t-1)$ is the previous value of the tumor highest temperature. Then, the error is:

$$e_{T,max} = T_{tumor,ref} - T_{max}(t+1) \tag{9}$$

where $T_{tumor,ref}$ is the target highest tumor temperature.

→ Future error in the surrounding healthy tissue temperature ($e_{T,healthy}$): In this case, Equation 8 is applied using the highest temperature in the healthy tissue region. Thus, the error is given by the following expression:

$$e_{T,healthy} = T_{healthy,ref} - T_{max_{healthy}}(t+1) \quad (10)$$

where $T_{healthy,ref}$ is the target highest healthy tissue temperature.
This temperature was assumed to be measured at no more than 2 mm from the tumor boundary.

Each of these error inputs were associated with their corresponding membership functions. The FLC output, or controlled signal, was the change in laser power (ΔP), and it was related to five membership functions. With these inputs and output defined, a Sugeno fuzzy interference system was implemented with a total of thirteen rules, presented on Table 1.

Table 1. Fuzzy logic rules used for the controller design.

$e_{TD,tumor}$	$e_{T,max}$	$e_{T,healthy}$	Operator	ΔP
P	VP	P	AND	VP
P	P	P	AND	P
P	0	P	AND	0
P	N	P	AND	N
P	VP	0	AND	0
P	P	0	AND	0
P	0	0	AND	0
P	N	0	AND	N
P	VP	N	AND	N
P	P	N	AND	N
P	0	N	AND	N
P	N	N	AND	N
0	VN	VN	OR	VN

Notes: VP = Very Positive, P = Positive, N = Negative, VN = Very Negative

This table could be summarized in three general rules that are followed **hierarchically** by the FLC:

(1) If the tumor thermal damage reaches the 100%, i.e, if $e_{TD,tumor}$ is zero, ΔP will be very negative (VN) until the laser is shut down (power equal to 0 W).
(2) If the healthy tissue temperature limit is exceeded, i.e., if $e_{T,healthy}$ is negative, the laser power will decrease this temperature is below the limit.
(3) The maximum tumor temperature can be considered as a desired ablation temperature for this work. Therefore, if none of the above conditions are met, the FLC will change the laser power to try to reach this desired ablation temperature ($e_{T,max} = 0$) without breaking any of the previous rules. This maximum temperature will be referenced as a setpoint from now on; however, it's important to remember that the above rules are hierarchically higher.

A saturation value was given to the laser power, so that the FLC did not request more than the maximum power of the laser used nor less than zero Watts. In this work, the maximum rate of temperature raise was not considered for the controller design.

The controller was implemented as a Sugeno FLC through MATLAB's Fuzzy Logic Toolbox. The FLC operating ranges were defined experimentally. This controller was tested considering a 4 W laser, which was more than enough to reach target temperatures; however, lasers with higher maximum power could be used if 4 W was not sufficient to reach the highest tumor thermal damage in a particular therapeutic procedure.

2.3 Simulation parameters

Simulation tests were carried out in MALTAB® using two Toolboxes and one open source code. First, *ValoMC* was used to simulate light propagation in tissue in 3D. Then, Fuzzy Logic Toolbox was utilized for the design and implementation of the FLC. Finally, Partial Differential Equation Toolbox was employed to simulate the thermal behavior of the tissue exposed to hyperthermia.

Furthermore, for the geometry, it was considered that laser source was external, in order to promote one of the main advantages of PTT, its minimal invasiveness. In consequence, four types of tissue were taken into account Hong et al. (2009a,b):

- Skin: More external layer with dimensions of 30 mm × 30 mm × 2 mm (HeightxLenghtxWidth).
- Subcutaneous fat: Layer between skin and muscle. Dimensions of 30 mm × 30 mm × 2 mm.
- Muscle: Deeper layer considered with dimensions of 30 mm × 30 mm × 26 mm.
- Tumor: The tumor was modeled as a superficial half-sphere of 10 mm in diameter, i.e., the equator of the hemisphere was located in the outermost part of the skin.

Table 2. Optical properties of simulated tissues. Recovered from Prahl1 (1999); Prahl (2017); Jacques (2013); Bashkatov et al. (2011); Ren et al. (2017).

Tissue	μ_a [cm^{-1}]	μ_s [cm^{-1}]	g	n
Skin	0.208	51.005	0.715	1.377
Subcutaneous fat	0.0835	37.083	0.715	1.44
Muscle	0.214	82.729	0.934	1.37
Tumor	0.214	167.756	0.934	1.37
Tumor with NRs	0.895	167.833	0.934	1.37

Table 3. Thermal properties of simulated tissues. Recovered from Wilson and Spence (1988); Lang et al. (1999).

Tissue	k [W/mK]	C_p [J/kgK]	ρ [kg/m^3]
Skin	0.53	3800	1200
Subcutaneous fat	0.16	850	2300
Muscle	0.53	3800	1270
Tumor	0.642	3500	1000

Optical and thermal properties of tissue considered for simulations are shown in Tables 2 and 3 respectively. Since gold nanorods (NRs) were considered to enhance optical absorption of the tumor tissue, in Table 2 coefficients are presented both for the tumor without and with NRs. The optical properties of NRs were determined assuming NRs with an effective radius of 11.43 nm and aspect ratio of 6.83. Also a volume fraction of 10^{-7} was employed. Tumor with NRs properties were calculated according to (Ren

et al., 2017). The optical properties were determined according to a laser wavelength of 1064 nm. The parameters A and ΔE_a from Equation 6 were set as shown in Table 4.

Table 4. The parameters A and ΔE_a for simulated tissues. Recovered from Paruch (2020).

Tissue	A [s^{-1}]	ΔE_a [J/mol]
Healthy tissue	$1.18x10^{44}$	$3.02x10^{5}$
Tumor	$1.98x10^{106}$	$6.67x10^{5}$

As already commented, maximum laser power was set to 4 W. The used conditions are:

(1) External boundary (in contact with ambient): natural convection with ambient temperature of 25 °C and heat transfer coefficient of 5 W/(m^2K) (Ren et al., 2017).
(2) Internal boundaries: isothermal with temperature of 37 °C (normal human body temperature).
(3) Initial condition: temperature of 37 °C for the whole tissue sample, corresponding to normal human body temperature.

3. SIMULATION RESULTS

Three tests were conducted to observe the FLC performance. The only difference between them was the value of the maximum temperature setpoint (**desired ablation temperature**) of the tumor ($T_{tumor,ref}$). The three values used were 60 °C, 70 °C and 80 °C. Maximum temperature limit of healthy tissue was set to 46 °C, which is already considered hyperthermia; however, near these temperature values, large amounts of time are required to generate considerable thermal damage. Because high hypethermia was expected to occur inside the tumor, the tumor ablation procedure had a short duration. The main objective was to reach complete tumor ablation, i.e., 100% of tumor thermal damage.

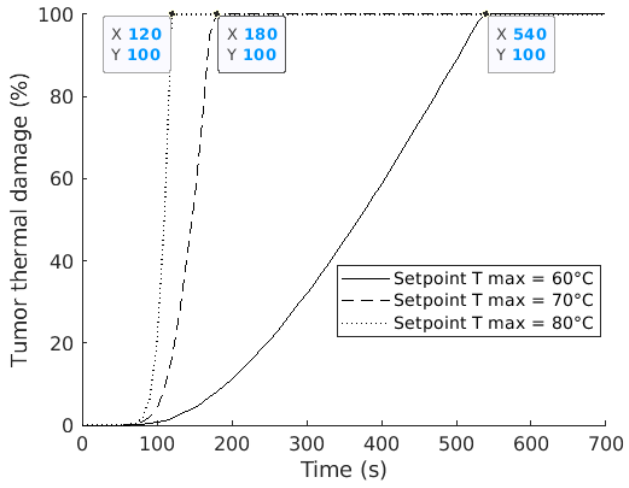

Fig. 1. Tumor thermal damage percentage. Obtained from simulations.

Complete tumor ablation was successful in the three cases simulated, as shown in Figure 1. As expected, when the desired ablation temperature is increased, thermal damage rate also boosts. Times required to achieve 100% damage were 540 s, 180 s and 120 s for maximum temperature setpoints of 60 °C, 70 °C and 80 °C, respectively. This time value changed abruptly when increasing the setpoint from 60 °C to 70 °C. This is because, for this particular tissue simulation, a parameter called *critical temperature* lies between 60 °C and 70 °C. The critical temperature is unique for each tissue and is defined as the temperature at which the thermal damage rate is 1 (Pearce, 2018). For the tumor simulated in this work, the critical temperature had a value around 54.61 °C; therefore, the proximity of the ablation temperature of 60 °C to the critical temperature makes the thermal damage rate for this case much slower than with setpoints of 70 °C and 80 °C. Knowing this parameter can help define the best temperature restrictions and PTT parameters, such as the desired ablation temperature ($T_{tumor,ref}$), according to the critical temperatures of both tumor and surrounding healthy tissue.

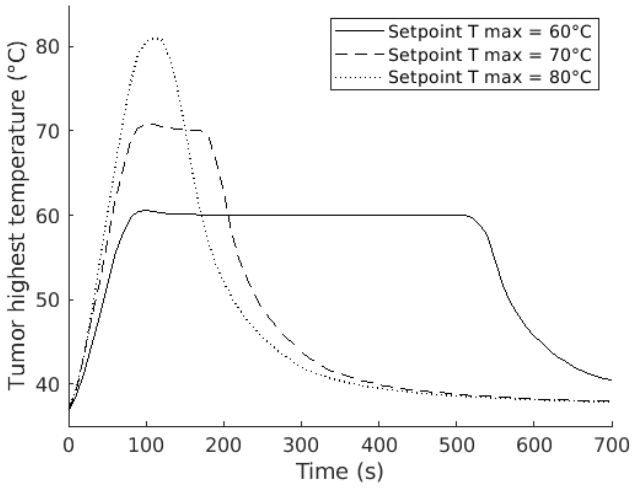

Fig. 2. Tumor highest temperature. Obtained from simulations.

Ablation temperature responses in the three cases simulated are shown in Figure 2. The settling times to 2% tolerance band were approximately 80 s when using both 60 °C and 70 °C as setpoints, and about 90 s for 80 °C. The maximum percentage overshoot (P.O.) did not exceed 1.3% in any of the instances, and the biggest value was obtained for the case of 80 °C. It's also important to notice that when considering a setpoint of 80 °C, the temperature is not maintained at 80 °C since the tumor thermal damage reaches the 100% first (see Figure 1).

Because thermal distribution is a slow process, the FLC sample time (i.e., time intervals at which FLC receives feedback from the system and defines the change in laser power) was set to 10 s; however, this parameter may need to be changed if thermal properties of tissue irradiated make thermal propagation faster or if the highest temperature limit is set above 80 °C.

In Figure 3, healthy tissue highest temperature responses are shown. It can be seen that only when using a setpoint of 80 °C for T_{max}, healthy tissue temperature exceeded its setpoint of 46 °C; however, it did not increase beyond

48 °C. This situation, together with the high critical temperature of all of the healthy tissue, caused that thermal damage in surrounding tissue was kept below 1%. Besides the reasons already discussed, the presented results show the importance of having information about of the critical temperature in order to determine the parameters as well as feasibility of using PTT according to thermal and optical properties of both tumor and neighboring healthy tissue.

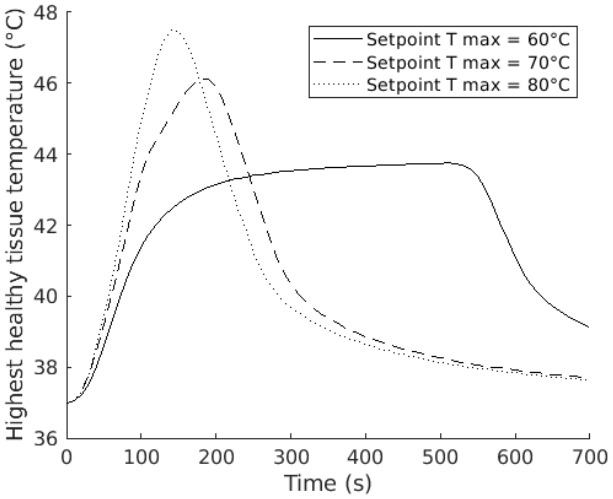

Fig. 3. Surrounding healthy tissue temperature. Obtained from simulations.

The results presented in this document do not aim to represent all possible clinical situations. The mathematical model of tissue implemented was used as a way to evaluate the FLC performance. Therefore, it might be necessary to readjust the controller parameters, such as the maximum allowable temperature in both healthy and tumor tissue, depending on the particular clinical case for which the system is used. Fuzzy logic controllers have the advantage of operating by rules that are more understandable to non-engineering professionals. One way to further improve the clinical feasibility of this controller is the development of a graphical user interface where clinicians can adjust the controller parameters according to their knowledge and real-time observations.

The controller was designed assuming there is a reliable real-time temperature measurement system, such as ultrasound or photoacoustic imaging, available as an input. The optimization of the temperature monitoring techniques is out of the scope of this work, and each technique may add additional limitations. Because of the possible errors that the controller and/or measurement system could have during the ablation procedure, the FLC presented here could also serve not as the direct controller of the laser power, but as a tool to help the physicians decide the most optimal laser power and to alert about possible undesired situations, such as irreversible thermal damage to healthy tissue, in real time.

4. CONCLUSION

The presented FLC successfully controlled laser power to achieve complete tumor ablation while avoiding the maximum the damage of surrounding healthy tissue. There are limitations in photothermal therapy, mainly related to light propagation in tissue. Therefore, future work should be focused in studying the application of the system in tissues with different characteristics in order to define relevant limitations, such as maximum tumor depth at which therapy is still successful. Future work will include the development of a graphical user interface (GUI) that would make the system usage easier for health care personnel. Additionally, other control algorithms could be implemented and tested along with the FLC presented here, using tissue-mimicking phantoms to assess the performance of the different controllers in a physical setting.

REFERENCES

Bashkatov, A.N., Genina, E.A., and Tuchin, V.V. (2011). Optical properties of skin, subcutaneous, and muscle tissues: A review. *Journal of Innovative Optical Health Sciences*, 4(1), 9–38. doi:10.1142/S1793545811001319.

Chen, H., Li, D., and Li, Z. (2019). Temperature feedback-controlled photothermal treatment based on thermal infrared imager. *Proceedings of SPIE*, (March 2019), 28. doi:10.1117/12.2507579.

Chen, W.R., Adams, R.L., Heaton, S., Dickey, D., Bartels, K.E., and Nordquist, R.E. (1995). Chromophore-enhanced laser-tumor tissue photothermal interaction using an 808-nm diode laser. *Cancer Letters*, 88(1), 15–19. doi:10.1016/0304-3835(94)03609-m.

Choy, V., Sadeghian, A., Sherar, M.D., and Whelan, W.M. (2002). Evaluation of a fuzzy logic controller for laser thermal therapy. *Laser Tissue Interaction XIII: Photochemical, Photothermal, and Photomechanical*, 4617(June 2002), 77–86. doi:10.1117/12.472510.

Chris Brace (2008). Thermal Tumor Ablation in Cinical Use. *IEEE Journal of Electromagnetics, RF and Microwaves in Medicine and Biology*, 23(1), 1–7. doi:10.1109/MPUL.2011.942603.Thermal.

Deenen, D.A., Maljaars, E., Sebeke, L., de Jager, B., Heijman, E., Grüll, H., and Heemels, W.P. (2018). Offset-free model predictive control for enhancing MR-HIFU hyperthermia in cancer treatment∗. *IFAC-PapersOnLine*, 51(20), 191–196. doi:10.1016/j.ifacol.2018.11.012.

Dombrovsky, L.A., Timchenko, V., Jackson, M., and Yeoh, G.H. (2011). A combined transient thermal model for laser hyperthermia of tumors with embedded gold nanoshells. *International Journal of Heat and Mass Transfer*, 54(25-26), 5459–5469. doi:10.1016/j.ijheatmasstransfer.2011.07.045.

Douplik, A. (2014). 10.09 - laser surgery. In A. Brahme (ed.), *Comprehensive Biomedical Physics*, 169 – 203. Elsevier, Oxford. URL http://www.sciencedirect.com/science/article/pii/B978044453632701011X.

Ge, X., Fu, Q., Bai, L., Chen, B., Wang, R., Gao, S., and Song, J. (2019). Photoacoustic imaging and photothermal therapy in the second near-infrared window. *New Journal of Chemistry*, 43(23), 8835–8851. doi:10.1039/c9nj01402k.

Hong, H.K., Jo, Y.C., Choi, Y.S., Park, H.D., and Kim, B.J. (2009a). An optical system to measure the thickness of the subcutaneous adipose tissue layer. In *SENSORS, 2009 IEEE*, 695–698. doi:10.1109/ICSENS.2009.5398349.

Hong, H.K., Jo, Y.C., Choi, Y.S., Park, H.D., and Kim, B.J. (2009b). An optical system to measure the thickness of the subcutaneous adipose tissue layer. *2009 IEEE Sensors*. doi:10.1109/icsens.2009.5398349.

Instituto Nacional del Cáncer (2011). El uso de la hipertermia en el tratamiento del cáncer. URL https://www.cancer.gov/espanol/cancer/tratamiento/tipos/cirugia/hoja-informativa-hipertemia.

International Agency for Research on Cancer (2003). Latest global cancer data: Cancer burden rises to 18.1 million new cases and 9.6 million cancer deaths in 2018. *Asian Pacific Journal of Cancer Prevention*, 4(1), 3–4.

Jacques, S.L. (2013). Optical properties of biological tissues: A review. *Physics in Medicine and Biology*, 58(11). doi:10.1088/0031-9155/58/11/R37.

Jacques, S.L. and Health, O. (1995). Monte Carlo Modeling of Light Transport in Tissues. In A.J. Welch and M.J. van Gemert (eds.), *Optical-Thermal Response of Laser-Irradiated Tissue*, chapter 4. Springer, 1 edition. doi:10.1007/978-1-4757-6092-7.

Jeraldin Auxillia, D. (2015). Automated system for ultrasound hyperthermia cancer treatment based on POF controller. *Biomedical Research (India)*, 26(4), 686–692.

Kengne, E., Lakhssassi, A., and Vaillancourt, R. (2012). Temperature Distribution in Living Biological Tissue Simultaneously Subjected to Oscillatory Surface and Spatial Heating: Analytical and Numerical Analysis. *International Mathematical Forum*, 7(48), 2373–2392. URL http://www.researchgate.net/publication/228328091_Temperature_Distribution_in_Living_Biological_Tissue_Simultaneously_Subjected_to_Oscillatory_Surface_and_Spatial_Heating_Analytical_and_Numerical_Analysis/file/d912f4ff7132aab099.pdf.

Lang, J., Erdmann, B., and Seebass, M. (1999). Impact of nonlinear heat transfer on temperature control in regional hyperthermia. *IEEE Transactions on Biomedical Engineering*, 46(9), 1129–1138. doi:10.1109/10.784145.

Leino, A.A., Pulkkinen, A., and Tarvainen, T. (2019). ValoMC: a Monte Carlo software and MATLAB toolbox for simulating light transport in biological tissue. *OSA Continuum*, 2(3), 957. doi:10.1364/osac.2.000957.

Long, S., Xu, Y., Zhou, F., Wang, B., Yang, Y., Fu, Y., Du, N., and Li, X. (2019). Characteristics of temperature changes in photothermal therapy induced by combined application of indocyanine green and laser. *Oncology Letters*, 17(4), 3952–3959. doi:10.3892/ol.2019.10058.

Manzoor, A.A. and Dewhirst, M.W. (2011). *Hyperthermia*, 1785–1791. Springer Berlin Heidelberg, Berlin, Heidelberg. doi:10.1007/978-3-642-16483-5_2915.

National Cancer Institute (2015). What is cancer? URL https://www.cancer.gov/about-cancer/understanding/what-is-cancer.

Nguyen, T.H., Park, S., Hlaing, K.K., and Kang, H.W. (2016). Temperature feedback-controlled photothermal treatment with diffusing applicator: theoretical and experimental evaluations. *Biomedical Optics Express*, 7(5), 1932. doi:10.1364/boe.7.001932.

Paruch, M. (2020). Mathematical modeling of breast tumor destruction using fast heating during radiofrequency ablation. *Materials*, 13(1). doi:10.3390/ma13010136.

Pearce, J. (2011). Mathematical models of laser-induced tissue thermal damage. *International Journal of Hyperthermia*, 27(8), 741–750. doi:10.3109/02656736.2011.580822.

Pearce, J. (2018). Irreversible Tissue Thermal Alterations: Skin Burns, Thermal Damage and Cell Death. *Theory and Applications of Heat Transfer in Humans*, 553–590. doi:10.1002/9781119127420.ch26.

Pennes, H.H. (1948). Analysis of Tissue and Arterial Blood Temperatures in Resting Human Forearm. *Journal of Applied Physiology*, 1(2), 93–122. doi:10.5005/jp/books/12678{_}10.

Prahl, S. (2017). URL https://omlc.org/spectra/water/.

Prahl, S.A. (1988). *Light transport in tissue*. The University of Texas at Austin, Austin, USA. doi:10.1364/ao.28.002216.

Prahl1, S. (1999). Optical absorption of hemoglobin. URL https://omlc.org/spectra/hemoglobin/.

Rehman, S. (2018). *An Overview of Cancer Treatment Modalities*. doi:10.5772/intechopen.76558.

Ren, Y., Qi, H., Chen, Q., and Ruan, L. (2017). Thermal dosage investigation for optimal temperature distribution in gold nanoparticle enhanced photothermal therapy. *International Journal of Heat and Mass Transfer*, 106, 212–221.

Shah, J., Aglyamov, S.R., Sokolov, K., Milner, T.E., and Emelianov, S.Y. (2008a). Ultrasound imaging to monitor photothermal therapy – feasibility study. *Optics Express*, 16(6), 3776. doi:10.1364/oe.16.003776.

Shah, J., Park, S., Aglyamov, S., Larson, T., Ma, L., Sokolov, K., Johnston, K., Milner, T., and Emelianov, S.Y. (2008b). Photoacoustic imaging and temperature measurement for photothermal cancer therapy. *Journal of Biomedical Optics*, 13(3). doi:10.1117/1.2940362.

Shaikh, T., Emrich, J., and Komarnicky-Kocher, L.T. (2013). *Hyperthermia*, 336–340. Springer Berlin Heidelberg, Berlin, Heidelberg. doi:10.1007/978-3-540-85516-3_6.

Soni, S., Tyagi, H., Taylor, R.A., and Kumar, A. (2015). The influence of tumour blood perfusion variability on thermal damage during nanoparticle-assisted thermal therapy. *International Journal of Hyperthermia*, 31(6), 615–625. doi:10.3109/02656736.2015.1040470.

Sun, L., Collins, C.M., Schiano, J.L., Smith, M.B., and Smith, N.B. (2005). Adaptive real-time closed-loop temperature control for ultrasound hyperthermia using magnetic resonance thermometry. *Concepts in Magnetic Resonance Part B: Magnetic Resonance Engineering*, 27(1), 51–63. doi:10.1002/cmr.b.20046.

VanBaren, P., Beck, E., Ebbini, E.S., and Cain, C.A. (1995). Feedback control of temperatures during hyperthermia treatments with phased-array ultrasound applicators. *Annual International Conference of the IEEE Engineering in Medicine and Biology - Proceedings*, 17(1), 613–614. doi:10.1109/iembs.1995.575276.

Wilson, S.B. and Spence, V.A. (1988). A tissue heat transfer model for relating dynamic skin temperature changes to physiological parameters. *Physics in Medicine and Biology*, 33(8), 895–912. doi:10.1088/0031-9155/33/8/001.